2018

Lattice parameter evolution during heating of Ti-45Al-7.5Nb-0.25/0.5C alloys under atmospheric and high pressures

Xi Li
University of Wollongong, Australian Nuclear Science and Technology Organisation, xl910@uowmail.edu.au

Rian J. Dippenaar
University of Wollongong, rian@uow.edu.au

Ayumi Shiro
National Institute for Quantum and Radiological Science and Technology

Takahisa Shobu
Japan Atomic Energy Agency

Yuji Higo
Japan Synchrotron Radiation Research Institute

See next page for additional authors

Lattice parameter evolution during heating of Ti-45Al-7.5Nb-0.25/0.5C alloys under atmospheric and high pressures

Abstract

Lattice strain evolution during deformation processing of Ti-Al alloys at high temperature is important in terms of its microstructural evolution and microstructural stability. It is shown here that careful evaluation of lattice parameters is critical for the understanding of thermal expansion, crystallographic order, chemical composition and response to pressure, allowing to identify phase transitions and segregation, in addition to the measurement of the more conventional quantities phase composition and order parameter. The lattice parameters of Ti-45Al-7.5Nb-0.25/0.5C (at. %) alloys were calculated using both Rietveld and single peak fitting methods from data obtained by in-situ synchrotron diffraction experiments at high temperature under atmospheric and high pressure respectively. The lattice strain evolution as a function of temperature in a Ti-45Al-7.5Nb-0.25C (at. %) alloy under high pressure was compared with that of a Ti-45Al-7.5Nb-0.5C (at. %) alloy heated under atmospheric pressure. The contribution of each of the four lattice strain factors is semi-quantitatively assessed in the temperature range investigated.

Disciplines

Engineering | Science and Technology Studies

Publication Details

Li, X., Dippenaar, R., Shiro, A., Shobu, T., Higo, Y., Reid, M., Suzuki, H., Akita, K., Funakoshi, K. & Liss, K. (2018). Lattice parameter evolution during heating of Ti-45Al-7.5Nb-0.25/0.5C alloys under atmospheric and high pressures. Intermetallics, 102 120-131.

Authors

Xi Li, Rian J. Dippenaar, Ayumi Shiro, Takahisa Shobu, Yuji Higo, Mark H. Reid, Hiroshi Suzuki, Koichi Akita, Ken-Ichi Funakoshi, and Klaus-Dieter Liss

Lattice parameter evolution during heating of Ti-45Al-7.5Nb-0.25/0.5C alloys under atmospheric and high pressures

Xi Li [a,b], Rian Dippenaar [a], Ayumi Shiro [c], Takahisa Shobu [d], Yuji Higo [e], Mark Reid [a,b], Hiroshi Suzuki [f], Koichi Akita [f], Ken-Ichi Funakoshi [g], Klaus-Dieter Liss [a,b,f,h,i*]

[a] School of Mechanical, Materials, Mechatronic and Biomedical Engineering, University of Wollongong, NSW 2522, Australia

[b] Australian Nuclear Science and Technology Organisation, Lucas Heights, NSW 2234, Australia

[c] Quantum Beam Science Research Directorate, National Institute for Quantum and Radiological Science and Technology, Kouto, Sayo, Hyogo 679-5148, Japan.

[d] Materials Sciences Research Center, Japan Atomic Energy Agency, Kouto, Sayo, Hyogo 679-5148, Japan.

[e] SPring-8, Japan Synchrotron Radiation Research Institute, Kouto, Sayo, Hyogo 679-5198, Japan.

[f] Materials Sciences Research Center, Japan Atomic Energy Agency, Tokai, Ibaraki 319-1195, Japan.

[g] Neutron Science and Technology Center, Comprehensive Research Organization for Science and Society (CROSS), Tokai, Ibaraki 319-1106, Japan.

[h] Guangdong Technion – Israel Institute of Technology, Shantou 515063, China.

[i] Technion – Israel Institute of Technology, Haifa 32000, Israel.

* Correspondence: kdl@gtiit.edu.cn, kdliss@technion.ac.il and liss@kdliss.de;

Abstract

Lattice strain evolution during deformation processing of Ti-Al alloys at high temperature is important in terms of its microstructural evolution and microstructural stability. It is shown here that careful evaluation of lattice parameters is critical for the

understanding of thermal expansion, crystallographic order, chemical composition and response to pressure, allowing to identify phase transitions and segregation, in addition to the measurement of the more conventional quantities phase composition and order parameter. The lattice parameters of Ti-45Al-7.5Nb-0.25/0.5C (at. %) alloys were calculated using both Rietveld and single peak fitting methods from data obtained by *in-situ* synchrotron diffraction experiments at high temperature under atmospheric and high pressure respectively. The lattice strain evolution as a function of temperature in a Ti-45Al-7.5Nb-0.25C (at. %) alloy under high pressure was compared with that of a Ti-45Al-7.5Nb-0.5C (at. %) alloy heated under atmospheric pressure. The contribution of each of the four lattice strain factors is semi-quantitatively assessed in the temperature range investigated.

Keywords: synchrotron radiation; TiAl; high pressure; high temperature; lattice strain

1. INTRODUCTION

Titanium aluminides are attractive candidate materials for applications in the automotive industry, and more importantly for applications at high temperature in aerospace industries, mainly due to their low density and excellent mechanical properties [1-3]. A new route for the processing of titanium aluminide components under high pressure has been proposed [4], for example, by utilizing a 0.8 GN forging press to manufacture large aerospace products [5] or a new 0.54 GN die-forging press currently being commissioned [6]. Since these forming processes operate at elevated temperature and pressure, it is imperative that the microstructural integrity of the work-pieces be maintained, especially by limiting grain growth during high-

temperature processing and minimizing the development of internal stresses during forging operations.

Processing in the ($\alpha_2/\alpha + \gamma$) phase-field remains a challenge due to crystalline anisotropy and the presence of intermetallic bonds. Appel *et al*. [7] pointed out that: "The important difference with alloys that solidify completely through β and those that subsequently precipitate α on further cooling, is that the α that forms from the β can do so with up to 12 different orientation variants". Thus, a large β grain can be divided into lamellar colonies with up to 12 different orientations. This effect, termed "crystal partitioning" [8, 9], can therefore lead to significant grain refinement of castings and significantly reduced texture. The β-phase is highly isotropic and independent slip systems can operate during dynamic recovery as experimentally confirmed by Liss *et al.* [10] in an *in-situ* synchrotron X-ray study. The β-solidifying alloys being studied in the present program have a fine and homogenous microstructure and are therefore easier to forge than conventional ($\alpha_2/\alpha + \gamma$) alloys [7, 11, 12]. It is possible to stabilize the β-phase by the addition of selected alloying elements, but it has recently been established that the β-phase can also be physically induced by the application of high hydrostatic pressure at high temperature. However, the question as to how this newly formed β-phase would affect the lattice strains in the α_2/α and γ phases has not been answered [13] and it is important to answer this question because the lattice strains have a determining influence on the mechanical properties of the product. Moreover, the evaluation of lattice parameters is a very sensitive measurement to determine phase transformations of various kinds [14-16] and can reveal segregation pathways in phase diagrams [17]. Therefore, under the aspect of lattice parameter evolution as the main complementary evaluation we re-

visit data from two *in-situ* heating experiments, to compare (i) a high-energy synchrotron radiation study on Ti-45Al-7.5Nb-0.5C under atmospheric pressure [16] with (ii) an energy-dispersive synchrotron X-ray diffraction experiment on Ti-45Al-7.5Nb-0.25C under high pressure at 9.6 GPa [13].

Figure 1(a) shows a section through the Ti-Al binary phase diagram [18], while a section through a Ti-Al-7.5 at. % Nb alloy, proposed by Chladil *et al*. [19] is shown in Figure 1(b). The alloy used in the present study is schematically shown by the vertical line at 45 at. % Al. It is important to note that this section through the phase diagram applies to atmospheric pressure and to the knowledge of the authors, the extent to which pressure changes the pertaining phase equilibria has not been determined as yet.

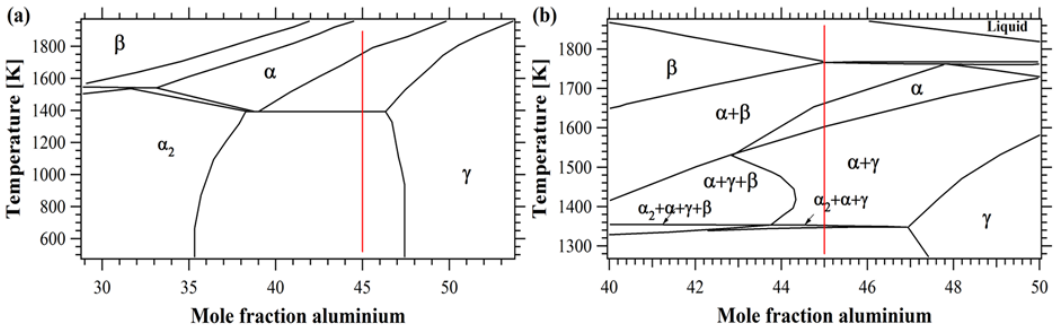

Figure 1. (a) Binary phase diagram of Ti-Al [18]; (b) Section through a proposed phase diagram of the Ti-Al-Nb alloy system for an alloy containing 7.5 at. % Nb [19].

Since we study a Ti-Al-Nb-C alloy under conditions of severe-plastic deformation and high temperature, it is important to identify the most critical parameters that determine microstructural evolution and stability. One important variable is lattice parameter evolution, since for example, a change in the *c*/*a* ratio of the α-lattice has a determining influence on the pertaining slip and twinning deformation mechanisms. Moreover, changes in the lattice parameter impact on orientation relationships and

have an influence on interphase stress development. In addition, the mechanism and morphology of phase transformations need to be taken into account since they play an important role in achieving microstructural stability.

Although the lattice parameter evolution plays a pivotal role in assessing the high-temperature behavior of titanium-aluminides, as argued above, only little information has been traced to date, with the notable exception of the *in-situ* studies early by Shull *et al.* [20], then by Yeoh *et al.* [21] and more recently that of Liss *et al.* [13].

The very early work of Shull *et. al* in 1990 reports on the first *in-situ* investigation of titanium aluminides at high temperature, focusing on the experimental determination of phase fields, while lattice parameter evolution is traced. In 2007, Yeoh *et al.* [21] reported the changes occurring in the *c*/*a* ratio of the lattice parameters in a Ti-45Al-7.5Nb-0.5C alloy during heating at atmospheric pressure. She suggested that as far as X-ray analyses are concerned, a simplification should be made by assuming that the α_2- (ordered) and the α-phase (disordered) be regarded as a single phase since X-rays cannot clearly distinguish between an ordered and disordered structure.

Liss *et al*. [13] recently conducted an *in-situ* X-ray diffraction experiment on a Ti-45Al-7.5Nb-0.25C alloy under high hydrostatic pressure. They studied the phase evolution of a Ti-45Al-7.5Nb-0.25C alloy as a function of time under high pressure and high temperature within a synchrotron X-ray source (SPring-8 beamline BL04B1, run number M1472). The *in-situ* diffactograms are displayed in Figure 2 which have been analyzed by the Rietveld method using MAUD (*Material Analysis Using Diffraction software* [22, 23]) for the evolution of phase fractions as a function of temperature, shown in Figure 3. Also shown are the phase fractions determined by Yeoh *et al.* [21] in a roughly similar alloy Ti-45Al-7.5Nb-0.5C, but under standard

atmospheric conditions. The two alloys have been manufactured under identical conditions and the two *in-situ* experiments were conducted under normal atmospheric and high pressure respectively. However, it is important to note that carbon can have a significant influence on phase evolution in these alloys and for this reason care need to be taken in comparing the alloys containing 0.25 at. % C and 0.5 at. % C respectively. For example, the eutectoid temperature, T_{eu} , is increased by 20 K from 1453 K to 1473 K, but the respective γ-solvus, $T_{\gamma,solv}$, 1565 K and 1566 K respectively [24] remains essentially constant. Notwithstanding these differences, the two alloys can be compared with respect to their respective pressure-induced behaviors. The *fcc*-based, ordered γ-phase of $L1_0$ structure, co-exists with an *hcp*-based, ordered α_2-phase of $D0_{19}$ structure at room temperature. Upon heating, the α_2-phase undergoes an inverse eutectoid order-disorder transition to form a fully disordered hexagonal α-phase at T_{eu}. The fraction of the γ-phase decreases upon heating and finally transforms fully into the disordered α-phase at $T_{\gamma,solv}$. Salient features when the Ti-45Al-7.5Nb-0.25C alloy is heated under a pressure of 9.6 GPa, are the appearance of the *bcc* β-phase in an $(\alpha + \alpha_2 + \beta + \gamma)$ field and the dissolution of γ phase at $T_{\gamma,solv}$ to form $(\alpha + \beta)$.

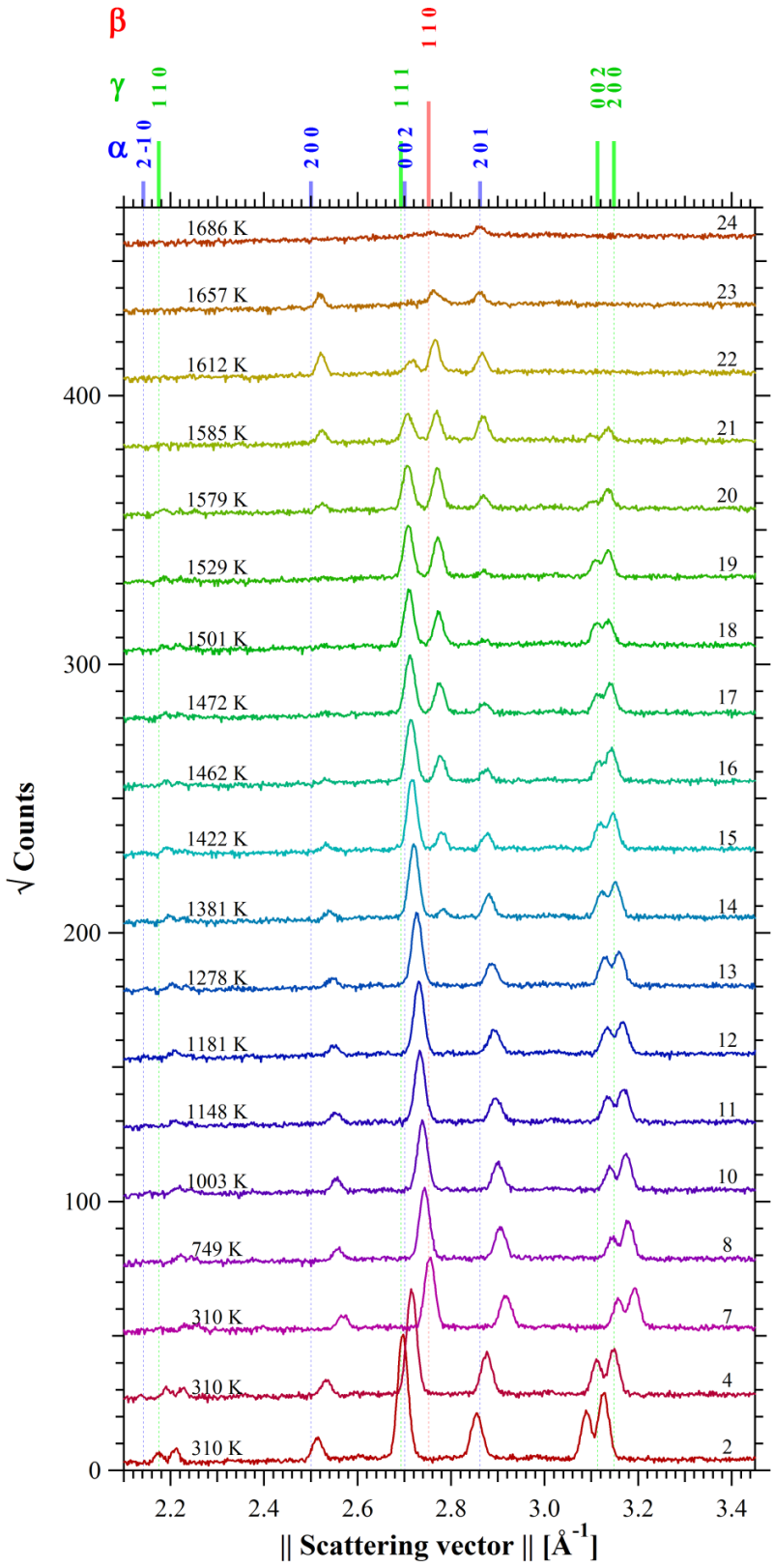

Figure 2. Measured diffraction patterns of a Ti-45Al-7.5Nb-0.25C alloy obtained under high pressure (9.6 GPa). Temperature tags are shown on the left and serial numbers on the right [13]. The first three patterns at 310 K were taken at pressures of 0, 3.2 and 9.6 GPa, respectively (based on [13] under CC-BY license).

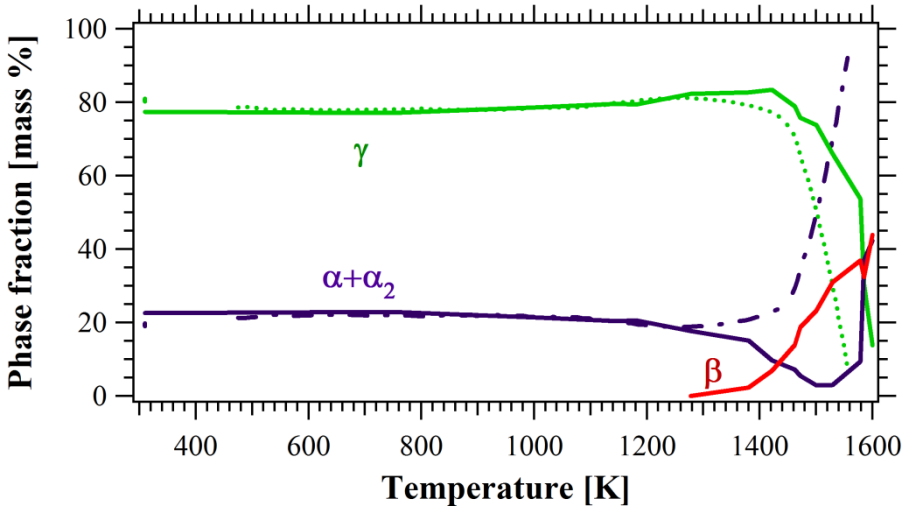

Figure 3. Phase evolution in a Ti-45Al-7.5Nb-0.25C alloy at a pressure of 9.6 GPa (continuous lines) (based on [13] under CC-BY license) compared with observations at standard atmospheric pressure (dotted lines) for a Ti-45Al-7.5Nb-0.5C alloy, replotted from Yeoh *et al.* [21].

Liss *et al.* [13] analyzed the lattice strain development in the Ti-45Al-7.5Nb-0.25C alloy at 310 K at three pressures, up to 9.6 GPa (series numbers 2, 4 and 7 in Figure 2). They calculated the changes in lattice parameter of the γ- and α_2/α-phases as a function of pressure at this temperature [13] and argued that at room temperature, the volume response to pressure is accommodated by the phase transformation $\gamma \rightarrow \alpha_2$, rather than by volumetric strain. They further determined some crystallographic aspects, specifically lattice strain and atomic order, at room temperature, but did not determine lattice strain evolution during heating at high pressure, which is subject of the current project. It is the dearth of information of this parameter, critical to processing at high temperature and pressure, which prompted the present investigation.

The overarching aim of the present work was the re-visit of the experimental data of

both experiments [13, 27] in order to compare the behavior of the selected alloys under atmospheric and high pressure respectively.

The specific aims were:

- to determine the lattice parameter evolution as a function of temperature at atmospheric pressure in the Ti-45Al-7.5Nb-0.5C alloy.
- to determine lattice parameter evolution as a function of temperature under high hydrostatic pressure in the Ti-45Al-7.5Nb-0.25C alloy.

It will be shown below that the experimentally determined lattice parameter evolutions occur in response to thermal expansion, alloy element segregation, order parameter and pressure. The specific trends and values will be decomposed based on an understanding of strain evolution with reference to the reported phase diagram at atmospheric pressure, before interpreting the evolution in the unknown system under high pressure. These new insights are opening new pathways to better understand structural transformations in the experimentally confined system. Such understanding is an essential element in optimizing the intended production techniques of titanium-aluminides since microstructural stability plays an important role in determining processing parameters.

2. EXPERIMENTS

Lattice strain evolutions were calculated from the raw data of two earlier experiments:

- Yeoh *et al.* [21] conducted *in-situ* high-energy X-ray diffraction studies under proposal number MA-77 at the ID15B beamline at the ESRF in Grenoble using a two-dimensional detector. They ramped up a Ti-45Al-7.5Nb-0.5C alloy from

184 room temperature to 1375 K at a rate of 5 K/min before ramping down to a rate of
185 2 K/min. Once a temperature of 1675 K was reached, it was maintained for 5
186 minutes before cooling down to room temperature at a rate of 5 K/min. All details
187 of the experiment have been described by Yeoh *et al.* [21].

188 ▪ Liss *et al.* [13] conducted *in-situ* X-ray diffraction studies at the BL04B1
189 beamline at the modern synchrotron source SPring-8 [25, 26] and a detailed
190 account of the experimental procedures is to be found in their paper [13]. Because
191 of the novelty in the field, it is pertinent to briefly refer to the most important
192 aspects of the experiment. They used a Kawai-type multi-anvil press, SPEED-
193 Mk.II, with a nominal maximum force of 15 MN. A pressure cell within an
194 integrated resistance-heating furnace was designed in order to provide the
195 capability of heating the specimen up to its melting point under a pressure of
196 9.6 GPa. Energy-dispersive X-ray diffraction with a beam size of $0.5 \times 0.7\ mm^2$
197 and a diffraction angle $2\theta = 5.9827°$ has been recorded by a 10 mm thick
198 germanium solid-state detector. The setup is limited to an effective diffraction
199 range of ~1.8 to 7.5 $Å^{-1}$. It is important to point out that a systematic experimental
200 error in the pressure can creep in during the *in-situ* experiment due to pressure
201 release at high temperature as a result of the softening of the anvil gasket material
202 (see section 3.2.3).

203 Both single peak fitting and Rietveld refinement, using the MAUD program, were
204 conducted to extract lattice parameters and phase fractions from the diffraction
205 patterns obtained in these two experiments. The *Igor Pro 4* software (WaveMetrix,
206 Lake Oswego, OR, USA) was then used to calculate the lattice strains and to perform
207 curve fitting.

The two titanium-aluminides of nominal chemical composition Ti-45Al-7.5Nb-0.25/0.5C used in the present study were produced by a powder metallurgical processing technique. Powder was manufactured by a plasma-melting induction-guiding atomization technique and consolidated by hot-isostatic pressing for 2 h at a pressure of 200 MPa and a temperature of 1553 K [27]. Both alloys were characterized by Chladil *et al.* [4, 24] and the resulting microstructure at room temperature consists of a globular γ-phase and lamellar (α_2 + γ) two-phase colonies [4].

While the experimental settings are described in the references, we like to raise an error estimate at this point, particularly to validate the later described lattice parameter fluctuations and features of the present manuscript. While the atmospheric pressure data in angle-dispersive setting appear as smooth curves, due to much faster and therefore finer sampling, the high-pressure data has been undertaken on temperature holding steps with larger step size, representing sometimes larger jumps between them, which could be interpreted as error fluctuations. Care has been undertaken by validating the realty of such jumps re-visiting the original data - i.e. looking out for changes of peak shape, overlapping etc and by the two kinds of fitting analysis both Rietveld and single peak. We come up with the following estimate of error, demonstrating the trend of the features we discuss on lattice strain evolution:

- For the high-pressure setup [13] the energy calibration based on fluorescence lines of Mo, Pb, Au, Ag, Pt, Ta and Cu and single peak fitting (see below) has been calibrated to and accuracy of ~1E-4. Subsequently, the diffraction angle was calibrated using MgO and Au as standard materials at ambient conditions.
- At 1278 K, the single Gaussian fitted absolute peak positions for the [γ-111, α_2-201] reflections are [2.73, 2.89] $Å^{-1}$ (we reproduce only 3 digits in this

text, however error propagation used full numerals) with an error of [5.49E-5, 1.8E-4] $Å^{-1}$ resulting in $\Delta G/G$ of [2.0E-5, 6.2E-5]. Similar results are obtained at 1612 K, also for the β-110 reflection with a value of $\Delta G/G$ = 3.9E-5.

- Moreover, we are interested in strain values rather than absolute values which propagates the errors and evaluates to double the $\Delta G/G$ uncertainties, resulting in about ~(1-2)E-4.
- Rietveld refinement reported inaccuracies of lattice parameter determinations as represented in the subsequent plots. They are mostly consistent with the error estimation by single peak fitting, however Rietveld error bars diverge for the α_2/α-phase around 1500 K because of the weakness of some of their peaks.

Note moreover, physically meaningful errors may originate from drifts in temperature or pressure, as it will be discussed further in the paper. We exclude significant drifts during a particular holding step, which would otherwise express in peak shape and broadening. Single-peak fitting of the α_2-201 reflection has been performed and confirms the trends with an error of ~3E-4, even in the range around 1500 K, allowing a qualitative interpretation of peak shifts due to various lattice variations, such as change of phase composition, disorder transformation etc, as it will be discussed.

3. RESULTS

3.1. Lattice strains at standard atmospheric pressure

The evolving lattice strains were calculated by equation (1),

$$\varepsilon = \varepsilon_{hkl} = (G_0 - G)/G_0 \quad (1)$$

For a given reflection, G_0 are the reciprocal lattice vectors at 300 K and G are the measured values at increasing temperature. The lattice strain discussed below is not an absolute lattice strain but is merely the difference in strain with respect to a reference value at 300 K. Lattice strains of the Ti-45Al-7.5Nb-0.5C alloy at standard

atmospheric pressure are shown in Figures 4 and 5 for the co-existing phases, α_2/α and γ, respectively. Both figures display an initial linear relationship between lattice strain and temperature which then evolves abnormally and anisotropically. Also shown is the average lattice strain, expressed as $\Delta V/3V$ of the atomic volume expansion ($\Delta V/V = 2\Delta a/a + \Delta c/c$), as a function of temperature. The changes in lattice strain can be divided into four distinct temperature regions, which we discuss for each phase.

3.1.1 The α_2/α-phase

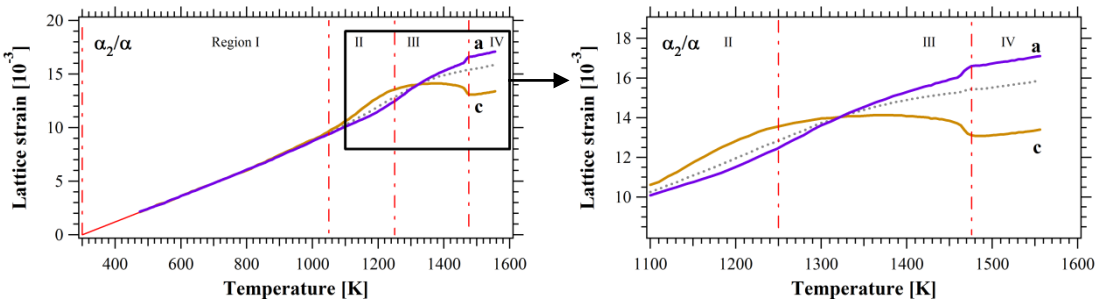

Figure 4. Dependence of the lattice strains in the α_2/α-phase along the *a*- and *c*-directions (purple and brown respectively) as well as 1/3 of volumetric expansion (dotted curve), as a function of temperature in a Ti-45Al-7.5Nb-0.5C alloy at standard atmospheric pressure.

In region I, strain evolution in both *a*- and *c*-directions is linear. In region II, the strains increase gradually to higher values than can be accounted for by linear thermal expansion alone. The lattice strain along the *a*-direction in region III increases more rapidly than in region II whereas it remains nearly constant along the *c*-direction, even under the influence of the counter-balanced thermal expansion. Region IV is characterized by a distinct kink in the strains of both lattice parameters at 1476 K [21], presumably as a result of the occurrence of the reverse eutectoid reaction $\alpha_2 \rightarrow$

α. Following these sudden changes, the strain increases gradually with an increase in temperature.

3.1.2 The γ-phase

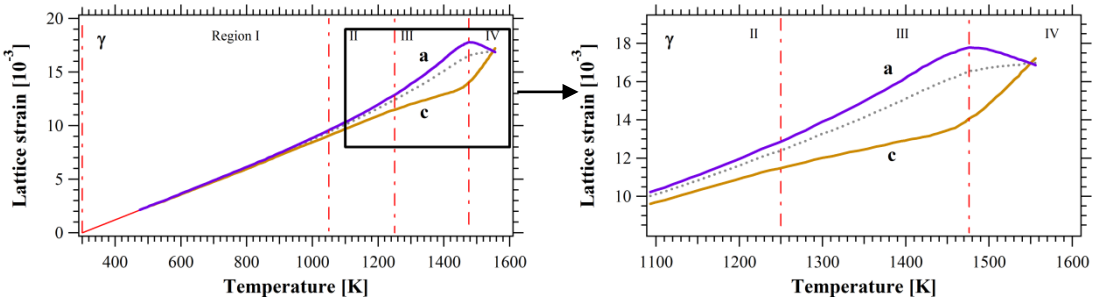

Figure 5. Lattice strains in the γ-phase along the *a*- and *c*-directions (purple and brown) as well as 1/3 of the volumetric expansion (dotted curve), as a function of temperature in a Ti-45Al-7.5Nb-0.5C alloy at standard atmospheric pressure.

The lattice strain evolution of the γ-phase is shown in Figure 5 in both the *a*- and *c*-directions, together with the weighted average (1/3 of the volumetric strain).

In region I, the strain evolution of the γ-phase is similar to that in the α_2/α-phase. In region II, the strain in both the *a*- and *c*-directions increases almost linearly since the dominant contributing factor to lattice strain is thermal expansion. In region III, the strain in the γ-phase along the *a*-direction increases up to T_{eu} whereas the strain in the *c*-direction increases to a lesser extent, developing significant anisotropy. In region IV, the strain in the *a*-direction decreases while the strain in the *c*-direction increases. The volumetric strain deviates only slightly from linearity and at the $T_{\gamma,solv}$ of 1565 K, all strain components meet as if they had expanded isotropically and linearly from room temperature.

3.2. Lattice strain at high pressure

The experimentally determined lattice strains of the α_2/α- and γ-phases are shown in Figures 6 and 7 for the Ti-45Al-7.5Nb-0.25C alloy under a pressure of 9.6 GPa. It is instructive to divide strain development into four regions.

Region I depicts the lattice strain evolution as a function of temperature in the range 300 K to 1003 K, where the α_2-phase has not yet reached thermodynamic equilibrium. Region II ranges from 1003 K to 1420 K ($T_{\gamma,max}$) and is divided into sub-regions II_a and II_b, separated by the appearance of the β-phase at 1350 K ($T_{\beta,start}$) [13]. Region III ranges from 1420 K to 1510 K (T_{eu}), while region IV covers the temperature range above 1510 K.

3.2.1 The α_2/α-phase

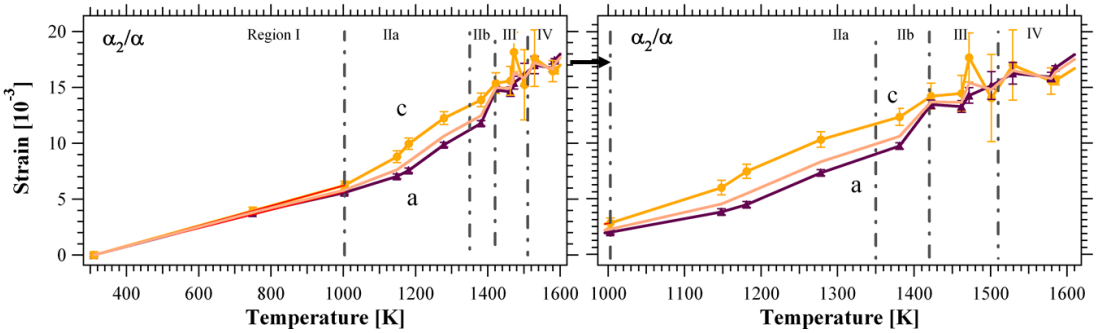

Figure 6. Lattice strains in the α_2/α-phase along *a*-(purple), *c*-(brown) directions and 1/3 of volumetric expansion (pink) as a function of temperature (K) for a Ti-45Al-7.5Nb-0.25C alloy at a nominal pressure of 9.6 GPa.

Figure 6 shows the lattice strain evolution of the α_2/α-phase along the *c*- and *a*-directions respectively. In region I, the lattice strain evolution is linear with respect to temperature. The strains along the *a*- and *c*-directions in region II increase more than

those in region I. In region II_b, the slope of the strain-temperature curve along the *a*-direction is higher than that along the *c*-direction, indicating a decrease in the *c/a*-ratio. A significant increase in strain occurs at 1420 K (the $T_{\gamma,max}$). In region III, a maximum value of the lattice strain along *c*-direction is noticed at 1472 K. In region IV, the lattice strain increases in the *a*-direction while there is an erratic behavior in the *c*-direction.

3.2.2 The γ-phase

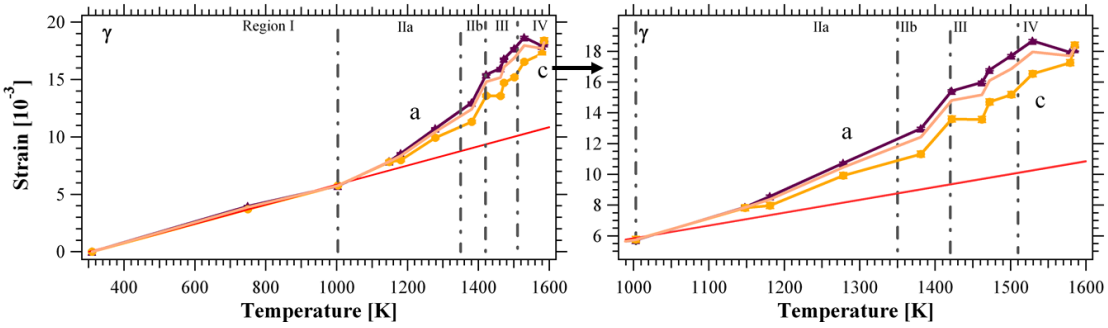

Figure 7. Lattice strain in the γ-phase along *a*- (purple), *c*- (brown) directions and 1/3 of volumetric expansion (pink curve) as a function of the temperature (K) for Ti-45Al-7.5Nb-0.25C at a nominal pressure of 9.6 GPa.

Figure 7 illustrates the lattice strain evolution of the γ-phase in the *a*- and *c*-directions, respectively. Noticeably, in region II_a, the strain increases more along the *a*-direction than in the *c*-direction, leading to a decrease of the *c/a*-ratio. In region II_b, the strain continues to increase but more so than in the previous region. In region III, the strain increases but not as steeply as in the region II_b. In region IV, the strain evolution trend is almost the same as under standard atmospheric pressure. The transformation temperatures T_{eu} and $T_{\gamma,solv}$ shift to higher temperatures at high pressure, evidenced by a comparison between Figures 5 and 7.

3.2.3 Experimental pressure release

During the experiments conducted at a hydrostatic pressure of 9.6 GPa, we have observed a progressive loss of sample pressure as a result of softening of the gaskets of the pressure cell at increasing temperature. Therefore, the sample pressure creeps down to about 6.9 ± 0.5 GPa over the time of the experiment, measured at 1473 K. This pressure loss of about 2.7 GPa has a marked effect on the absolute value of the measured crystal strain. In order to estimate the extent to which this pressure creep affects the quantitative values of the measured strain, we conducted the following analysis:

Experiments conducted at standard atmospheric pressure show that the volumetric lattice expansion increases linearly with temperature as shown in Figures 4 and 5. However, when the experiments are conducted at high pressure, there is a significant deviation from linearity to larger strain values, as shown in Figures 6 and 7. This deviation is illustrated in Figure 7 where the red line shows the extrapolation of linear thermal expansion.

There is clearly a significant difference between this expected linear dependence of lattice strain development as a function of temperature and the experimentally observed volumetric values (pink curve). We believe that this deviation is not due to differences in lattice strain, but is caused by thermally induced softening of the gaskets of the pressure cell as outlined above. Under atmospheric pressure, the linear extrapolation of thermal expansion meets closely the point of volumetric strain at $T_{\gamma,\mathrm{solv}}$, as shown in Figures 4 and 5. In order to assess this premise, we measured the difference in strain between the extrapolated linear thermal expansion and the average strain expressed by 1/3 volumetric strain (red and pink lines in Figure 7) at a

363 temperature of 1579 K as 0.00702. Since the value of the bulk modulus is known, 152
364 GPa [13], we used the relation $\partial p = -K \cdot \partial V/V$ to calculate the pressure difference
365 as 3.20 GPa. This calculated value of pressure release is in reasonable agreement with
366 the experimentally measured decrease of 2.7 GPa in pressure measured following the
367 heating cycle, thereby providing evidence that the observed deviation can indeed be
368 attributed to the sample pressure release as a result of a leak in the seal of the pressure
369 cell. The two pressure release values are particularly in good agreement taking into
370 account that only the room temperature bulk modulus is available.
371 The values of strain shown in Figure 7 are therefore higher than the true values of
372 lattice strain under 9.6 GPa by up to 25% and the isotropic lattice strain as a result of
373 temperature change has to be estimated. However, the anisotropic part, as will be
374 discussed later, is well representative.

375 **4. DISCUSSION**

376 In order to better understand how changes in lattice parameter influence
377 microstructural evolution, account has to be taken of the factors contributing to such
378 lattice strains. When the temperature increases, the strains in both crystallographic *a*
379 and *c* directions increase, while an increase in the aluminium content in the respective
380 phase results in a decrease in those strains. The order parameter is defined as $S = \frac{p-r}{1-r}$,
381 where p is the probability that an atom resides in the ordered position r (The
382 concept of the order parameter is discussed in more detail in the Appendix). The order
383 parameter is a measure of the anisotropic behavior: when either the α_2- or γ-phase
384 develops an ordered structure, the strain along the *a*-direction decreases whereas that
385 along the *c*-direction increases. A summary of the influence of the order parameter in
386 the different temperature regions, is shown in Figures 8, 9, 11 and 13. It is to be noted

that these figures only show the trend in strain (the exact quantitative strain values haven't been shown).

4.1. Lattice strains at standard atmospheric pressure

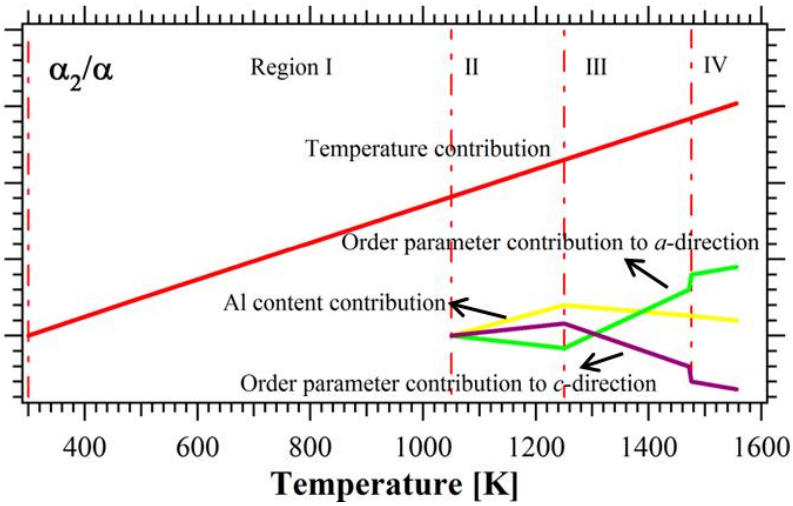

Figure 8. Factors contributing to lattice strain evolution in the α_2/α-phase at standard atmospheric pressure.

Figure 8 shows how temperature, aluminium content and the order parameter affect strain evolution of the α_2/α-phase under standard atmospheric pressure. It is pertinent to discuss these observations:

Region I: lattice strain increases linearly with respect to temperature because the dominating contributing factor is thermal expansion, which, for most solids is proportional to the temperature change ΔT, with $\varepsilon_{thermal} = \eta \cdot \Delta T$ [28], where η is the linear thermal expansion coefficient. Region II: It is reasonable to assume that the high-temperature equilibrium concentration of aluminium has been 'frozen' into the alloy during manufacturing. This means that the aluminium concentration in α_2 is

effectively higher than the equilibrium concentration at room temperature. With an increase in temperature, long-range diffusion of aluminium becomes possible, such that the α_2-phase is depleted in aluminium, effectively meaning that the titanium concentration in the α_2-phase increases. Higher concentrations of titanium lead to an increase in atomic volume [13] and hence, accounts for the observed increase in lattice strain as a function of temperature. Region III: The curvature of lattice strain evolution in the α_2/α-phase along the *a*- and the *c*-direction has different signs. This observation is ascribed to the occurrence of an order-disorder transformation (the order-disorder transformation is discussed in more detail in the appendix). Region IV: Both lattice strains ε_a and ε_c show a distinct, respectively positive and negative step change at the boundary of regions (III) and (IV), coinciding with a sharp decrease in order parameter (see Figure A.2, Appendix). It is important to note that the volume strain evolves smoothly, without a step-change. This observation provides evidence of the premise that the change of order does not affect the atomic volume, but only strain anisotropy.

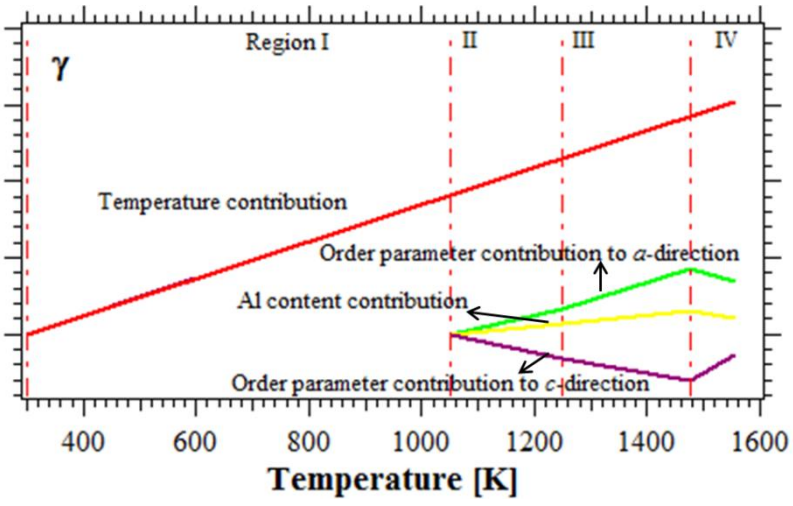

Figure 9. Factors contributing to lattice strain evolution in the γ-phase at atmospheric pressure.

Figure 9 shows how temperature, aluminium content and the order parameter affect strain evolution in the γ-phase at standard atmospheric pressure.

The thermal expansion is linear in region I along the *a*- and *c*- directions due to the linear temperature contribution. The small and anisotropic deviation from linearity in Region II is due to the extent to which aluminium contributes to the disordering of the TiAl-structure. It is observed that the lattice strain along the *a*-direction increases faster than along the *c*-direction, and since the *c*-dimension is larger than the *a*-dimension, the unit cell approaches more closely an *fcc* unit cell, that of a fully disordered γ-phase, revealing a higher degree of disorder and hence, a smaller order parameter. Witusiewicz *et al.* [29] have shown earlier that the aluminium concentration decreases well below stoichiometry in this temperature range as a function of temperature and that the lowest aluminium concentration in the γ-phase is attained at 1476 K, contributing to chemical disorder. Above 1476 K (in region IV), the aluminium content in the partially ordered γ-phase increases, as shown in Figure 10(a). Yeoh *et al.* [21] have shown that the *c*/*a* ratio decreases sharply with increasing temperature in Region III as shown in Figure 10(b). Hence, the strain along the *a*-direction increases more than in the *c*-direction and the TiAl-structure becomes highly disordered. In region IV, the *c*/*a* ratio increases sharply as shown in Figure 10(b) and the fully ordered TiAl-structure is approximated, due to the highest ordering energy of the γ-phase, compared to all other Ti-Al configurations [30].

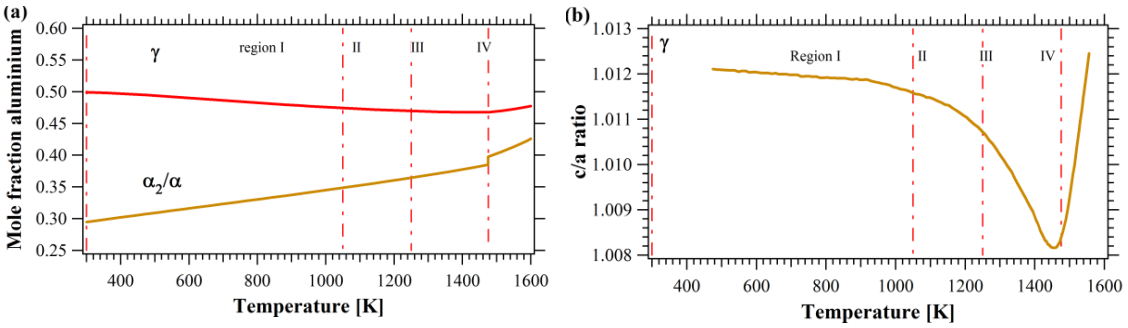

Figure 10: (a) Aluminium concentrations of the γ- and α_2/α-phases as a function of temperature as dereived from the phase diagram [29], (b) The *c*/*a* ratio of the α_2/α-phase for a Ti-45Al-7.5Nb-0.5C alloy at standard atmospheric pressure [21].

4.2. Lattice strains at high pressure

Figure 11 shows the trend in the strain evolution by the respective contributions of temperature, aluminium content in the respective phases, order parameter and pressure in the different regions for the α_2/α-phase at a nominal pressure of 9.6 GPa. In order to avoid bias from the experimental pressure release, we calculate the anisotropic part of strain ($\Delta a/a - \Delta V/3V, \Delta c/c - \Delta V/3V$) as shown in Figure 12 for the α_2/α-phase. The main features of the strain evolution of the α_2/α-phase at 9.6 GPa are illustrated as follows:

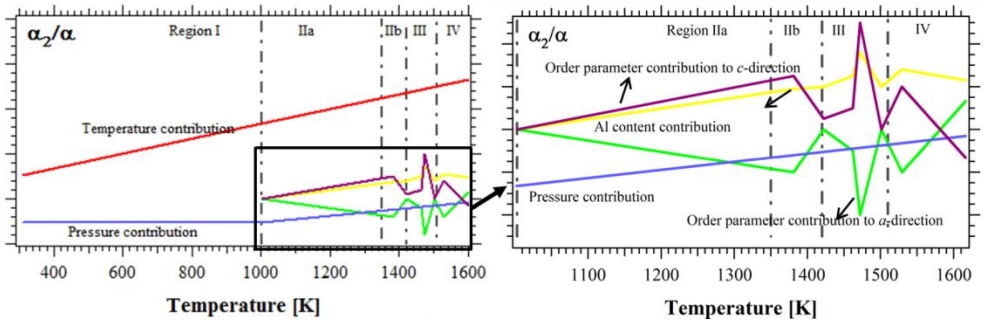

Figure 11. Contributors to strain evolution of the α_2/α-phase at nominal pressure of 9.6 GPa

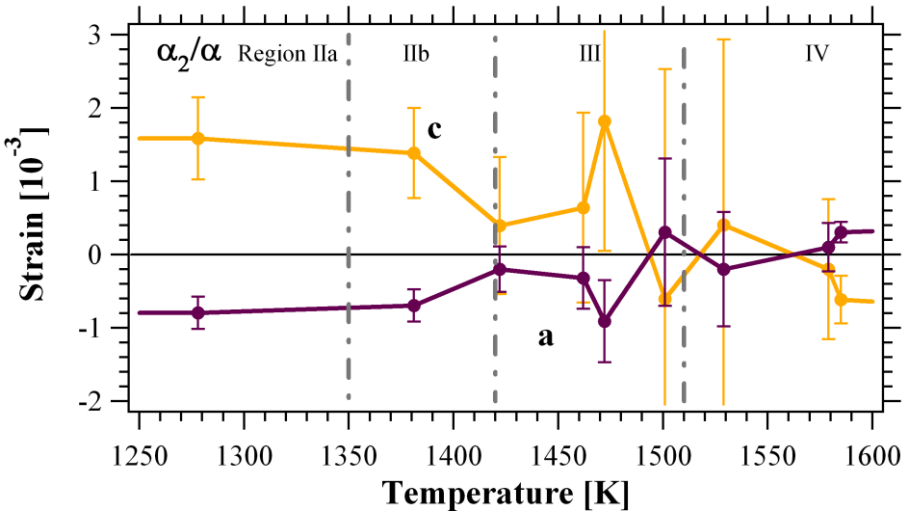

Figure 12. Anisotropic lattice strains of the α_2/α-phase along the *a*- (purple) and *c*- (brown) directions for the Ti-45Al-7.5Nb-0.25C alloy at 9.6 GPa

In region II_b the anisotropic strain increases in the *a*-direction and decreases in the *c*-direction. These observations are attributed to the order-disorder transition in the α_2/α-phase. In region III, the β-phase exists. The strain evolution under a pressure of 9.6 GPa is in the opposite direction in the temperature range 1420 K to 1472 K than observed under standard atmospheric conditions at the beginning of region III (see Figure 4). There is a steep increase along the *c*-direction between 1462 K and 1472 K, corresponding to the increase of the β-phase fraction (see Figure 3). The β-phase in solid solution has a *bcc* structure and provides an opportunity for the co-existing α_2-phase to drive closer to stoichiometry and order, increasing its *c*/*a* ratio. Moreover, under the assumption that β orders to β_0 with a B2 structure, the latter would extract Al from α_2, again emphasizing a higher degree of order in the latter. The transformation to β leads to a sharp decrease in the aluminium content of the supersaturated α_2/α-phase and hence, the α_2/α-phase is increasingly ordered. The change in the fraction of β-phase has a major influence on the aluminium

concentration in the α_2/α-phase from region III onwards. These arguments explain why the trend of the anisotropic strain in the α_2/α-phase correlate well with the β-phase evolution. By contrast, the main contributor is a thermally driven $\alpha \rightarrow \alpha_2$ order-disorder transition in region III under standard atmospheric pressure. The maximum value of anisotropic strain along the *c*-direction at 1472 K is probably driven by the appearance of an ordered β_0-phase, leading to a lower aluminium content in the α_2/α-phase. Under a pressure of 9.6 GPa, 1510 K, as a minimum of α-phase fraction, is taken as eutectoid temperature, reported by Liss *et al.* [13]. It indicates that under high pressure the eutectoid temperature would be increased. On approach to 1510 K, the order-disorder transition $\alpha \rightarrow \alpha_2$ occurs, the order parameter of the α_2/α-phase decreases, which results in the strain in the α_2/α-phase along the *c*-direction having a dramatic decrease. In region IV, up to 1529 K, the β-phase fraction increases sharply (Figure 3), leading to a trend of an increase along the *c*-direction and a decrease in *a*-direction in the α_2/α-phase, although questioned by large error bars. At higher temperature, the anisotropic strain along the *a*-direction increases while that along the *c*-direction decreases.

Figure 13 shows how temperature, aluminium content, order parameter and pressure contribute to strain evolution in the γ-phase at a nominal pressure of 9.6 GPa in the different regions respectively. Because of this observed pressure loss, the anisotropic part of strain, $(\Delta a/a - \Delta V/3V, \Delta c/c - \Delta V/3V)$ of the γ-phase is shown in Figure 14. The sample pressure is from 9.6 GPa to 6.9 GPa – a very similar order of magnitude which would not considerably change the phase transformation behavior. Moreover, this anisotropic part of lattice strain is subtracted by the pressure influence, but relevant features with respect to order parameter can be extracted. The significant

jumps in lattice parameter are definitely linked to phase transformations and not to pressure release. The main features of the strain evolution in the γ-phase at a nominal pressure of 9.6 GPa are discussed below:

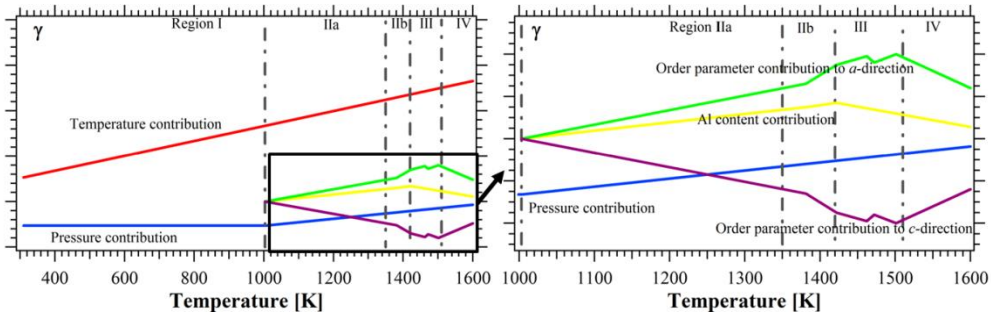

Figure 13. Contributors to strain evolution of the γ-phase at nominal pressure of 9.6 GPa

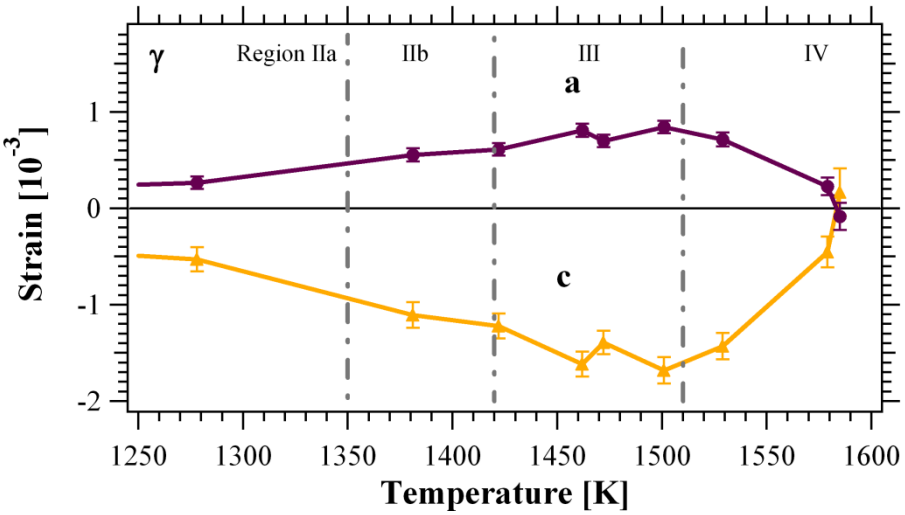

Figure 14. Dependence of the anisotropic lattice strain in the γ-phase along *a*- (purple), *c*- (brown) directions for Ti-45Al-7.5Nb-0.25C at 9.6 GPa

In region III, the transition of γ → α → β + α [13] results in an increased aluminium content in the γ-phase, therefore, the strain increase is lower compared to atmospheric pressure. The kink at 1472 K is attributed to the order parameter increase as a result of the fact that the γ-phase fraction decreases sharply in the temperature range 1462 to 1472 K. In region IV, the trend in strain evolution is almost the same as at

519 atmospheric pressure, since the main contributing factor is the order parameter.

520 **4.3. Phase sequence at high pressure**

521 Based on our experimental observations and the Rietveld analyses outlined above, a
522 new version of the sequence of phase changes occurring in the Ti-Al-7.5Nb-0.25C
523 alloy under a pressure of 9.6 GPa, is shown in Figure 15 in the region of the alloy
524 composition (delineated by the area between the two vertical dotted lines). This is the
525 first experimental evidence suggesting that during heating under high pressure the
526 sequence of phase development is $\alpha_2+\gamma$, $\alpha_2+\alpha+\gamma$, $\alpha_2+\alpha+\gamma+\beta$, $\alpha+\gamma+\beta$, $\alpha+\beta$, $L+\alpha+\beta$, $L+\beta$
527 and liquid L. Compared to the phase diagram suggested by Chladil *et al*. [19], it is
528 evident that the temperature range of the phase field $\alpha_2+\alpha+\gamma+\beta$ is extended under the
529 influence of a pressure of 9.6 GPa.

530

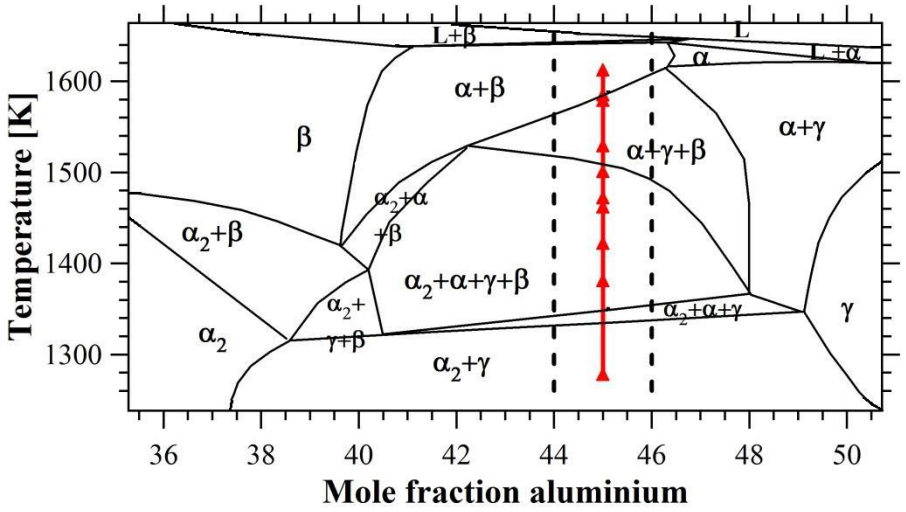

531

532 Figure 15. Proposed sequence of phase changes upon heating a Ti-Al-7.5 Nb-0.25C alloy under a
533 pressure of 9.6 GPa. The red triangles are based on the calculations of this study from the diffractions
534 measured by Liss *et al.* [13], superimposed on a section of a schematic diagram of the phase
535 compositions in the Ti-Al-7.5Nb-0.25C system.

536

4.4. Comparison of the observations at low and high pressure

The quantitatively calculated contributions to strain evolution at standard atmospheric pressure are listed in Table 1.

Table 1. Contribution to strain evolution at standard atmospheric pressure

Phase	Strain direction	Expansion coefficient η [10^{-6} K^{-1}]	Increasing Al content [10^{-6} mol^{-1}]	Atomic order S (0→1) [10^{-6}]
α_2/α	*a*	⇑ 12.075	⇓	⇓-695
	c	⇑ 12.047	⇓	⇑ 1390
	V/3	⇑ 12.066	⇓ -18959	⇔
γ	*a*	⇑ 12.412	⇓	⇓-4677*
	c	⇑ 11.847	⇓	⇑ 9420*
	V/3	⇑ 12.224	⇓-24079	⇔

* Computed with lattice parameter values of Beaven [31]

The linear thermal expansion coefficients are $\eta_a = 12.075 \cdot 10^{-6}\ K^{-1}$ and $\eta_c = 12.047 \cdot 10^{-6}\ K^{-1}$ for α_2/α-phase and $\eta_a = 12.412 \cdot 10^{-6}\ K^{-1}$ and $\eta_c = 11.847 \cdot 10^{-6}\ K^{-1}$ for γ-phase. They were extracted by fitting the curves of *a*- and *c*- directions in region I of Figures 4 and 5, since thermal expansion is proportional to the temperature change for most solids, $\varepsilon_{thermal} = \eta \cdot \Delta T$ [28, 32]. In order to calculate the contribution of the aluminium content of the α_2/α-phase, the slope of the strain (Figure 4 and Figure 5) and the slope of the phase boundary lines (Figure 10(a)) in region IV were used since the thermal expansion and the aluminium content both contribute to volumetric strain evolution in this region. The contribution of aluminium to the lattice strains

553 are $\partial\varepsilon/\partial C|_{\alpha} = -18959\cdot10^{-6}$ mol^{-1} and $\partial\varepsilon/\partial C|_{\gamma} = -24079\cdot10^{-6}$ mol^{-1} respectively, in good
554 agreement with the values reported by Dubrovinskaia *et al.* [33]. It should be noted
555 that the thermal expansion coefficient at high temperature will differ from the values
556 obtained by diffraction, as further factors may contribute, such as the creation of
557 lattice vacancies which do not change the lattice plane spacing but the length and
558 volume of a specimen. The order parameter contributions are $\partial\varepsilon/\partial S_a = -695\cdot10^{-6}$ and
559 $\partial\varepsilon/\partial S_c = 1390\cdot10^{-6}$ for α_2/α-phase along *a*- and *c*- directions respectively. The
560 experimental data points around the γ-solvus at 1476 K, were chosen to calculate
561 $\partial\varepsilon/\partial S$ for each component. In Figure 4, the steps across these data are $0.45\cdot10^{-3}$ and
562 $0.5\cdot10^{-3}$ for *a*- and *c*- directions respectively, which are recorded as $\Delta\varepsilon_a^M$ and $\Delta\varepsilon_c^M$
563 below. Considering that $\Delta\varepsilon_a^M$ and $\Delta\varepsilon_c^M$ are not only influenced by the order parameter,
564 but also by volume expansion, these equations were modified as follows:

565 $$\Delta\varepsilon_a = \Delta\varepsilon_a^M - \Delta\varepsilon_v,$$

$$\Delta\varepsilon_c = \Delta\varepsilon_a^M - \Delta\varepsilon_v$$

566 where $\Delta\varepsilon_v$ represents the slope of the average expansion, i.e. 1/3 of the volume
567 expansion curve. From Figure A.3, the slope of the order parameter (ΔS) across this
568 step is 0.456, resulting in $\partial\varepsilon/\partial S_a = \Delta\varepsilon_a/\Delta S = -695\cdot10^{-6}$ and $\partial\varepsilon/\partial S_c = \Delta\varepsilon_c/\Delta S =$
569 $1390\cdot10^{-6}$. The order parameter of the γ phase was estimated in a different way, since
570 no order parameter nor site occupation have been evaluated by Yeoh *et al.* [21]. The
571 fully disordered γ-phase would be *fcc* with a *c*/*a* axis ratio of one, and the atomic
572 volume is conserved during the order-disorder phase change. The lattice parameters of
573 the stoichiometric alloy have been reported by Beaven and Pfullman [31] and
574 extracted as $a_{50} = 4.0176$ Å and $c_{50} = 4.0745$ Å, for the fully ordered crystal structure.

$$a_{fcc} = \sqrt[3]{a_{50}{}^2 \times c_{50}}$$

leading to a_{fcc} = 4.03648 Å. When the crystal structure changes from a disordered (S = 0) to a fully ordered structure (S = 1), the influence of the structure parameter on strain development is calculated as $\partial\varepsilon/\partial S_a = (a_{50} - a_{fcc})/\, a_{fcc} = -4677 \cdot 10^{-6}$ and $\partial\varepsilon/\partial S_c = (c_{50} - a_{fcc})/a_{fcc} = 9420 \cdot 10^{-6}$, respectively.

Table 2 lists quantitative contributions to the strain evolutions at high pressure. The thermal expansion coefficients are calculated by linear curve fitting based on the strains in region I (Figures 6 and 7). They are $\eta_a = 8.126 \cdot 10^{-6}\ K^{-1}$, $\eta_c = 9.030 \cdot 10^{-6}\ K^{-1}$ for the α_2/α-phase and $\eta_a = 8.371 \cdot 10^{-6}\ K^{-1}$, $\eta_c = 8.359 \cdot 10^{-6}\ K^{-1}$ for γ-phase. The expansion coefficients are approximately $8 \times 10^{-6}\ K^{-1}$ under a compressive pressure of 9.6 GPa whereas it is $12 \times 10^{-6}\ K^{-1}$ under atmospheric pressure. Hence, a compressive pressure of 9.6 GPa decreases the expansion coefficient to 67% of the value at atmospheric pressure. An increase of aluminium content in the respective phases would lead to a decrease in the strain along the *a*- and *c*- directions, as well as a decrease in the volumetric strain. The application of an applied compressive pressure caused the strain to decrease in both phases. Liss *et al.* [13] has already calculated the strain decrease in the α_2/α-phase per 1 GPa is $2266 \cdot 10^{-6}$ along *a*-direction and $2189 \cdot 10^{-6}$ along the *c*-direction from the same experimental data. The corresponding strain decrease in the γ-phase is $2206 \cdot 10^{-6}$ along *a*-direction and $2293 \cdot 10^{-6}$ in the *c*-direction [13].

Table 2. Contributions to strain evolution at high pressure

Phase	Strain direction	Expansion coefficient	Increasing Al	Pressure*

		η [10^{-6} K^{-1}]	content	[10^{-6} GPa^{-1}]
α_2/α	*a*	⇑ 8.126	⇓	⇓ 2266
	c	⇑ 9.030	⇓	⇓ 2189
	V	⇑ 8.427× 3	⇓	⇓ 2240 × 3
γ	*a*	⇑ 8.371	⇓	⇓ 2206
	c	⇑ 8.335	⇓	⇓ 2293
	V	⇑ 8.359× 3	⇓	⇓ 2235 × 3

596 *Calculations by Liss *et al.* [13]

5. CONCLUSIONS

Lattice strain evolution in a Ti-45Al-7.5Nb-0.5C and a Ti-45Al-7.5Nb-0.25C alloy respectively was determined by *in-situ* experiments using high-energy X-rays at synchrotron storage rings. The temperature dependence of lattice strain evolution of the Ti-45Al-7.5Nb-0.5C alloy was studied at atmospheric pressure while the lattice strain evolution in a Ti-45Al-7.5Nb-0.25C was determined as a function of temperature under a compressive pressure of 9.6 GPa.

- Lattice strain evolution is determined by thermal expansion, changes in the aluminium content of the respective phases and the extent to which the respective phases are ordered under atmospheric pressure. Their interaction and respective quantitative values to lattice strain changes have been obtained, which provides valuable data to predict strain evolution in the future.

- Pressure has a determining influence on strain evolution in the alloys. A consequence of this finding is that the magnitude of the lattice strain can be manipulated by these four factors during manufacture. Hence, inter-granular stresses can be reliably predicted, minimized and controlled in order to manipulate the mechanical properties of candidate titanium aluminide alloys.

- The application of high pressure increases the eutectoid temperature T_{eu} and the temperature at which the transformation of the γ-phase is completed, $T_{\gamma,solv}$. The linear thermal expansion coefficient of the alloy investigated is about 1/3 (4×10^{-6} K^{-1}) lower under a pressure of 9.6 GPa, than under standard atmospheric pressure.

- Based on the experimental observations, a new version of the sequence of phase changes occurring at high pressure is proposed and illustrated with reference to a schematic phase diagram. This portion of the phase diagram shows that under high pressure, the $\alpha_2+\alpha+\gamma+\beta$ phase field is stabilized over a wide range of temperature.

- Lattice strains can be used to indicate the occurrence of phase transformations and changes in composition, which are otherwise difficult to determine.

- The *c*/*a* ratio of both the α_2/α- and γ- phases provides valuable insight into the extent to which these phases are ordered (as assessed by the order parameter).

- A discontinuity in the *c*/*a* ratio is an indication of the order-disorder transition $\alpha_2 \rightarrow \alpha$.

The present findings are of generic importance with respect to lattice parameter evaluation and are relevant to a multitude of intermetallic systems.

6. Acknowledgments

The authors are grateful for the financial contributions made by the China Scholarship Council (CSC), The University of Wollongong and the Australian Nuclear Science and Technology Organization (ANSTO). The provision of and access to experimental equipment at beamline BL04B1, SPring-8 (under proposal number 2013B1157) and the availability of data from experiment MA-77 taken at ID15A, ESRF and their experimentalists [21] are gratefully recognized. Dr. habil. Arno Bartels, Technische Universität Hamburg-Harburg, Germany, is acknowledged for providing the alloys used in this study.

7. Appendix

The concept of an order-parameter was introduced by Bragg and William [34]. They defined an order parameter S as follows:

$$S = \frac{p-r}{1-r} \qquad \text{Eq. (A.1)}$$

where p is the probability that an atom resides in an ordered position r. For example, if an aluminium atom remains in its ordered position (the red sites depicted in Figure A.1) and no other atoms occupy these positions, the value of p is 1. r is the fraction of aluminium atoms residing in a fully ordered lattice. The structure of a fully ordered lattice α_2-Ti_3Al is shown in Figure A.1. Aluminium atoms occupy 25% of the lattice positions, which means that r has a value of 0.25.

The order-disorder transition refers to the case where aluminium and titanium atoms in the crystal lattice randomly interchange anti-sites. For example, titanium atoms have the possibility of residing in red positions.

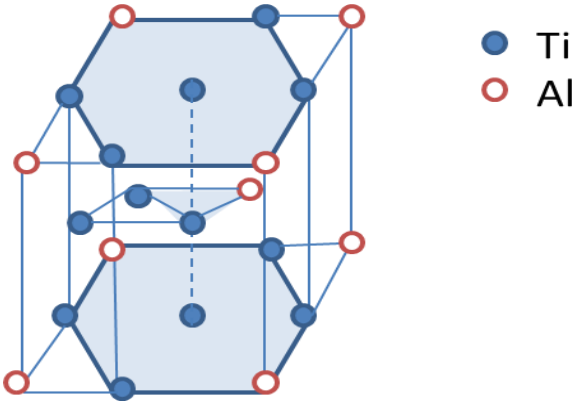

Figure A.1 the structure of ordered lattice α_2 phase (Ti_3Al)

Figure A.2 shows the order parameter (S) for the α_2/α-phase, calculated from the site

occupancies reported by Yeoh *et al*. [21] (without taking into account the change in aluminium concentration). The sharp decrease in order parameter coincides with the sudden change in the lattice strain shown in Figure 5. This observation indicates that a higher *c*/*a* ratio reflects a more ordered structure. It is instructive to compare the occurrence of this sudden change in order parameter to changes in the *c*/*a*-ratio of the α_2/α-phase as a function of temperature, as shown in Figure A.3. The order parameter changes in the same fashion as the *c*/*a* ratio in the α_2/α-phase and hence, it seems reasonable to use the *c*/*a* ratio as a measure of the degree to which the α_2/α-phase is ordered.

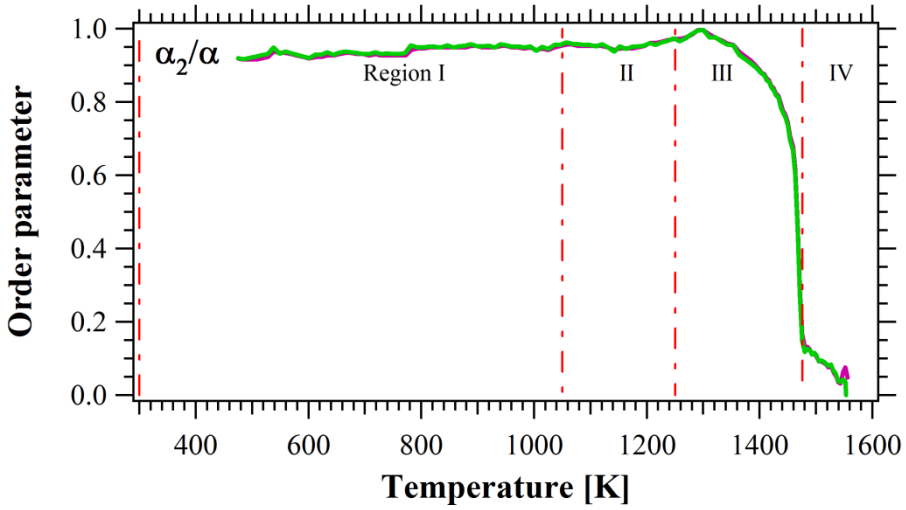

Figure A.2. The order parameter S for the α_2/α-phase at atmospheric pressure [21].

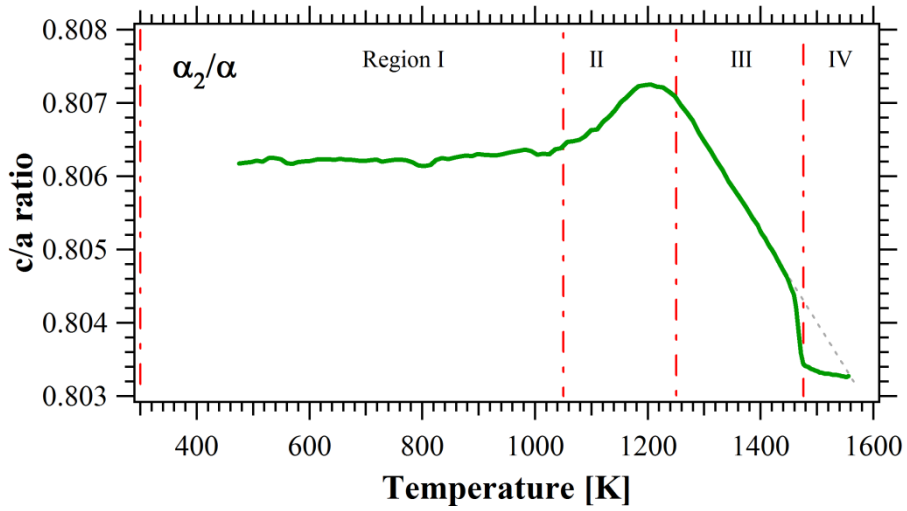

673

674 Figure A.3. The *c*/*a* ratio of the α_2/α-phase for a Ti-45Al-7.5Nb-0.5C alloy at atmospheric pressure
675 [21].

676

677 **8. References**

[1] R. Yang, "Advances and challenges of TiAl base alloys," *Acta Metallurgica Sinica,* vol. 51, 2015.

[2] K. H. Matucha, "Materials Science and Technology: a Comprehensive Treatment. Vol. 8. Structure and Properties of Nonferrous Alloys," *VCH Verlagsgesellschaft mbH, P. O. Box 10 11 61, Weinheim, D-69451, Germany, 1996. 837,* 1996.

[3] Y.-W. Kim, "Ordered intermetallic alloys, part III: gamma titanium aluminides," *Jom,* vol. 46, pp. 30-39, 1994.

[4] H. F. Chladil, H. Clemens, G. A. Zickler, M. Takeyama, E. Kozeschnik, A. Bartels*, et al.*, "Experimental studies and thermodynamic simulation of phase transformations in high Nb containing γ-TiAl based alloys," *International Journal of Materials Research,* vol. 98, pp. 1131-1137, 2007.

[5] FRANCE-METALLURGIE. (2014). *80,000 tons World's Largest Closed Die Forging Press help to develop China Jet Fighter J-11 (US)*. Available: http://www.france-metallurgie.com/china-80000-tons-world-s-largest-closed-die-forging-presses-help-to-develop-the-f-11-us/

[6] FRANCE-METALLURGIE. (2016). *OTTO FUCHS orders 54,000 Tons Closed Die Forging Press from SMS (US)*. Available: http://www.france-metallurgie.com/otto-fuchs-orders-54000-tons-closed-die-forging-press-from-sms-us/

[7] F. Appel, J. D. H. Paul, and M. Oehring, *Gamma titanium aluminide alloys: science and technology*: John Wiley & Sons, 2011.

[8] K. Khan, C. Sanchez, M. Thomas, S. Naka, and -. C. Office National d'Etudes et de Recherches Aerospatiales "Development of third generation castable gamma titanium aluminides: role of solidification paths," 1997.

[9] Y. Jin, J. N. Wang, J. Yang, and Y. Wang, "Microstructure refinement of cast TiAl alloys by β solidification," *Scripta Materialia,* vol. 51, pp. 113-117, 7// 2004.

[10] K.-D. Liss, T. Schmoelzer, K. Yan, M. Reid, M. Peel, R. Dippenaar*, et al.*, "In situ study of dynamic recrystallization and hot deformation behavior of a

multiphase titanium aluminide alloy," *Journal of Applied Physics,* vol. 106, p. 113526, 2009.

[11] H. Clemens and S. Mayer, "Design, processing, microstructure, properties, and applications of advanced intermetallic TiAl alloys," *Advanced Engineering Materials,* vol. 15, pp. 191-215, 2013.

[12] H. Clemens, M. Schloffer, E. Schwaighofer, R. Werner, A. Gaitzenauer, B. Rashkova*, et al.*, "Advanced β-Solidifying Titanium Aluminides–Development Status and Perspectives," in *MRS Proceedings*, 2013, pp. 3-16.

[13] K.-D. Liss, K.-I. Funakoshi, R. Dippenaar, Y. Higo, A. Shiro, M. Reid*, et al.*, "Hydrostatic Compression Behavior and High-Pressure Stabilized β-Phase in γ-Based Titanium Aluminide Intermetallics," *Metals,* vol. 6, p. 165, 2016.

[14] K.-D. L. Tapan Chatterji, and Thomas Tschentscher, "Anomalous Thermal Expansion Due to Magnetism in EuAs3 and MnS2," *ESRF Highlights,* 1997.

[15] T. Chatterji, K. Liß, G. McIntyre, M. Weiden, R. Hauptmann, and C. Geibel, "The ground state of NaV2O5," *Solid state communications,* vol. 108, pp. 23-26, 1998.

[16] K.-D. Liss, A. Bartels, A. Schreyer, and H. Clemens, "High-energy X-rays: a tool for advanced bulk investigations in materials science and physics," *Textures and Microstructures,* vol. 35, pp. 219-252, 2003.

[17] K. Yan, D. G. Carr, S. Kabra, M. Reid, A. Studer, R. P. Harrison*, et al.*, "In Situ Characterization of Lattice Structure Evolution during Phase Transformation of Zr‐2.5 Nb," *Advanced Engineering Materials,* vol. 13, pp. 882-886, 2011.

[18] J. C. Schuster and M. Palm, "Reassessment of the binary aluminum-titanium phase diagram," *Journal of phase equilibria and diffusion,* vol. 27, pp. 255-277, 2006.

[19] H. F. Chladil, H. Clemens, H. Leitner, A. Bartels, R. Gerling, and W. T. Marketz, "Experimental Studies of Phase Transformations in a Carbon Containing Ti‐45Al‐7.5 Nb Alloy and Related Thermodynamic Simulations," *Advanced Engineering Materials,* vol. 7, pp. 1131-1134, 2005.

[20] R. D. Shull and J. P. Cline, "High temperature X-ray diffractometry of Ti-Al

alloys," in *Materials Chemistry at High Temperatures*, ed: Springer, 1990, pp. 95-117.

[21] L. A. Yeoh, K.-D. Liss, A. Bartels, H. Chladil, M. Avdeev, H. Clemens*, et al.*, "In situ high-energy X-ray diffraction study and quantitative phase analysis in the α+ γ phase field of titanium aluminides," *Scripta Materialia,* vol. 57, pp. 1145-1148, 2007.

[22] L. Lutterotti, "Total pattern fitting for the combined size–strain–stress–texture determination in thin film diffraction," *Nuclear Instruments and Methods in Physics Research Section B: Beam Interactions with Materials and Atoms,* vol. 268, pp. 334-340, 2010.

[23] L. Lutterotti, S. Matthies, and H. Wenk, "MAUD (Material Analysis Using Diffraction): a user friendly Java program for Rietveld texture analysis and more," in *Proceeding of the twelfth international conference on textures of materials (ICOTOM-12)*, 1999, p. 1599.

[24] H. Chladil, H. Clemens, H. Leitner, A. Bartels, R. Gerling, F.-P. Schimansky*, et al.*, "Phase transformations in high niobium and carbon containing γ-TiAl based alloys," *Intermetallics,* vol. 14, pp. 1194-1198, 2006.

[25] Y. T. a. Y. Higo, "BL04B1: In situ observation of high pressure phase change of simple material," Spring-8, Kouto, Kyogo, Janpan, Tutorial 4Sep. 2007

[26] T. Katsura, K.-i. Funakoshi, A. Kubo, N. Nishiyama, Y. Tange, Y.-i. Sueda*, et al.*, "A large-volume high-pressure and high-temperature apparatus for in situ X-ray observation,'SPEED-Mk. II'," *Physics of the Earth and Planetary Interiors,* vol. 143, pp. 497-506, 2004.

[27] R. Gerling, H. Clemens, and F. P. Schimansky, "Powder Metallurgical Processing of Intermetallic Gamma Titanium Aluminides," *Advanced Engineering Materials,* vol. 6, pp. 23-38, 2004.

[28] F. Abe, T.-U. Kern, and R. Viswanathan, *Creep-resistant steels*: Elsevier, 2008.

[29] V. Witusiewicz, A. Bondar, U. Hecht, and T. Y. Velikanova, "The Al–B–Nb–Ti system: IV. Experimental study and thermodynamic re-evaluation of the binary Al–Nb and ternary Al–Nb–Ti systems," *Journal of Alloys and Compounds,* vol. 472, pp. 133-161, 2009.

[30] M. Asta, D. de Fontaine, and M. Van Schilfgaarde, "First-principles study of phase stability of Ti–Al intermetallic compounds," *Journal of materials research,* vol. 8, pp. 2554-2568, 1993.

[31] P. Beaven and T. Pfullmann, "Stoichiometry effects in TiAl and TiAlCr alloys," *Journal of materials science & technology,* vol. 10, pp. 321-330, 1994.

[32] O. A. Bauchau and J. I. Craig, *Structural analysis: with applications to aerospace structures* vol. 163: Springer Science & Business Media, 2009.

[33] N. Dubrovinskaia, M. Vennström, I. Abrikosov, R. Ahuja, P. Ravindran, Y. Andersson*, et al.*, "Absence of a pressure-induced structural phase transition in Ti 3 Al up to 25 GPa," *Physical Review B,* vol. 63, p. 024106, 2000.

[34] W. L. Bragg and E. J. Williams, "The effect of thermal agitation on atomic arrangement in alloys," *Proceedings of the Royal Society of London. Series A, Containing Papers of a Mathematical and Physical Character,* vol. 145, pp. 699-730, 1934.